ELSEVIER

Journal of Molecular Catalysis A: Chemical 168 (2001) 123–138

JOURNAL OF MOLECULAR CATALYSIS A: CHEMICAL

www.elsevier.com/locate/molcata

Lower order atomic multipole moments of the oxygen atoms of "small size" H-form aluminosilicate frameworks

A.V. Larin [a], D.P. Vercauteren [b,*]

[a] *Laboratory of Molecular Beams, Department of Chemistry, Moscow State University, Vorob'evu Gory, B-234 Moscow 119899, Russia*
[b] *Laboratoire de Physico-Chimie Informatique, Institute for Studies in Interface Sciences, Facultés Universitaires Notre Dame de la Paix, Rue de Bruxelles 61, B-5000 Namur, Belgium*

Received 26 April 2000; received in revised form 6 July 2000; accepted 12 October 2000

Abstract

The geometries of all possible Si–O(H)–Al Brönsted centres within five hydrogen form (H-form) aluminosilicate frameworks, ABW, CAN, CHA, EDI, and NAT, were optimised using a full periodic ab initio Hartree–Fock LCAO scheme at the STO-3G level. A distributed multipole analysis (DMA) was then applied at the ps-21G*(Al, Si)/6-21G*(O, H) level in order to obtain the multipole moments. Simple analytical approximations of the dependence of the Mulliken charges and atomic dipole moments with respect to the average bond distance, the anisotropy between the Al–O and Si–O distances, and the Si–O–Al angle for all crystallographically independent types of oxygen atom were derived on the basis of all optimised models. The nuclear quadrupole coupling constants for ^{17}O are calculated for all oxygen positions and compared to the experimental values measured for zeolites A, LSX, and Y.

Keywords: H-forms; Aluminosilicates; Brönsted centre

1. Introduction

Hydrogen forms (H-forms) of numerous sieves and zeolites are important active catalysts largely used in industrial scale MTG and MTO processes, catalytic cracking, etc. [1]. The understanding of the location and geometry of the Brönsted acid sites responsible for these applications is thus crucial to create new and more active catalysts. In this spirit, it was recently shown that the OH frequency, one of the important parameters of the H acidity, correlates well with the electrostatic field at the H position for both the silicoaluminophosphates (SAPO) and aluminosilicate forms [2]. The electrostatic interactions within the H-forms of these materials in the absence of cations, due to the usually shielded Si and Al atoms, are mainly governed by O atoms. If, however, the charge values can be estimated with an approach, such as Sanderson's electronegativity equalisation principle [3], a precise representation of the electrostatic field within zeolites merely requires the knowledge of the higher order multipole moments [4].

Precise electrostatic field values within a framework can be computed using the approximated distributed multipole analysis (DMA) scheme based on the atomic positions as proposed by Saunders et al. [4]. Such a scheme has been implemented in the CRYSTAL95 [5] ab initio Hartree–Fock LCAO code developed to tackle periodic systems. Saunders et al. [4] showed that a precision for the electrostatic field values below 1% using atomic moments up to the fourth order could be reached. Unfortunately, a

* Corresponding author. Fax: +32-81-72-45-30.

1381-1169/01/$ – see front matter
PII: S1381-1169(00)00493-3

periodic Hartree–Fock (PHF) solution cannot be obtained for systems with non-ordered positions of the T substituting atoms, where T = Al, P, Ga, B, Be, etc., or when the number of atoms per elementary unit cell (UC) is relatively large.

Other theoretical methods such as Hartree–Fock or density functional theory applied to isolated clusters [6] and plain wave approaches applied to a whole crystal [7] have already yielded geometries close to those from experiment for the Brönsted acid sites within the H-chabazite zeolite (HCHA). This system is often considered as a model one because of its reasonable size in terms of the number of crystallographically independent types of atom. However, if the local properties could be easily estimated using cluster models, the preferential H occupation of the different zeolite O sites should be interpreted together with a precise estimate of the long range interactions between the proton and the whole framework. An alternative explanation [8] compared to the one presented in [2] for the stabilisation of each proton being due to the size and shape of the zeolite cages, is that it could also be related to the different electrostatic interactions within each cavity and channel. This means that the most precise determination of the electrostatic field within zeolite frameworks remains a very important task, for which a PHF approach as developed in CRYSTAL may offer clear advantages.

In order to avoid the problem of the field computation for disordered and "very large" zeolite frameworks (in terms of the number of atoms per UC), several simple approximations of the multipole moments with respect to the internal co-ordinates (bond lengths, bond angles, etc.) were already derived for a series of zeolites and aluminophosphates (ALPO) with a relatively small number of atoms per UC [9–12]. In these previous studies, such approximations were sought for the Mulliken charges on the Si and O atoms within 13 all-siliceous zeolites [9–12] and for the charges on the Al, P, and O atoms (together with the dipole moment values for O) within a series of 12 ALPOs with the ratio Al/P = 1 [12].

Clearly, similar types of function should now also be sought for the H-forms of the zeolites, considering in these cases that an appreciable variation of the Si–O–Al geometry, because of the replacement of a cation by a proton, should be taken into account. Unfortunately, due to the irregular locations of the proton sites, the three-dimensional geometries of these H-forms cannot be obtained from X-ray diffraction (XRD) data, and thus necessitates the application of NMR spectroscopy, often together with theoretical approaches, in order to estimate the bond distances and angles of the bridged H moieties.

Useful information about the characteristics of the zeolite oxygens has indeed been recently provided by measurements of the ^{17}O chemical shift by solid state NMR [13–15]. Four band peaks in the ^{17}O double rotation (DOR) and dynamic angle spinning (DAS) NMR spectra of all-siliceous faujasite were recorded in accordance with the four O types in Y zeolite [13]. The interpretation of the four band peaks was done with the help of cluster type calculations. The distances obtained between the peaks corresponding to the four O types were qualitatively close those from experiment. However, all chemical shifts of the oxygens were overestimated, as well as their quadrupole coupling constants as compared to the experimental data. Subsequently, a correlation was experimentally demonstrated between the chemical shift and the Si–O–Al angle within low silicon zeolites (NaLSX and NaA, ratio Al/Si = 1) [15].

The perspectives of the application of CRYSTAL for the interpretation of the solid state NMR spectra look attractive in light of the determination of the electrostatic field gradient (EFG) based on XRD data. The resulting information from XRD is indeed limited by the orientation of the EFG tensor relative to the crystallographic axes. Brown and Spackman [16] clearly showed that the XRD interpretation failed if the EFG values and asymmetry of the EFG components are required. The PHF approach implemented in CRYSTAL provides a more precise estimation of these data [5].

The aim of this paper is, thus, to estimate the dependence of the multipole moments on the internal co-ordinates (bond distances, bond angles, etc.) as well as the EFG tensor components of the O atoms in a series of H-form aluminosilicates. In Section 2, we will shortly present the adopted computational strategy. The main features of the optimised models are discussed in Section 3.1. Sections 3.2 and 3.3 are devoted to the presentation of the results of the approximations of the atomic O charge and dipole (absolute value). In the last section, we discuss the nuclear quadrupole coupling constants, the EFG, and EFG anisotropy of

Table 1
Symbol, number of atoms of different Al, Si, and O types ($n_H = n_{Al}$), of atomic orbitals (AO) per unit cell (UC) (with ps-21G* basis), and symmetry group of the H-form aluminosilicates

Name	Symbol	Reference	Atoms/UC	$n_{Al}/n_{Si}/n_O$	AO/UC	Symmetry group
ABW	HABW	[18]	28	1/1/4	348	$Pna2_1$
Cancrinite	HCAN	[19]	42	1/1/4	527	$P6_3$
Chabazite	HCHA	[20]	39	1/3/8	517	$R3c$
Edingtonite	HEDI	[21]	34	1/2/5	430	$P2_12_12$
Natrolite	HNAT	[22]	34	1/2/5	430	$Fdd2$

the quadrupolar ^{17}O nuclei for the considered zeolites with comparison with the available experimental data.

2. Computational strategy

The theoretical bases for the solution of the Schrödinger electronic problem in three-dimensions considering periodic boundary conditions have already largely been described in the literature [5,17]. The optimisation of the partial co-ordinates of the Brönsted centre, i.e. the Si–O(H)–Al moiety, has been performed for a series of five aluminosilicates, ABW [18], CAN [19], CHA [20], EDI [21], and NAT [22] (Table 1), using the CRYSTAL95 code [5]. In Table 1, symmetry groups for all initial cationic forms mean non-equivalent Al and Si positions; this avoids a decrease in symmetry when replacing a cation by a bridged H atom. For all five frameworks, the variations of the co-ordinates of the four (O, H, Si, Al) framework atoms involved in each type of bridged Brönsted centre (12 variables) was allowed. The cell parameters were kept fixed as it was shown that their influence on the final geometry was of lower significance [7]. Only one bridged OH group per UC was considered at a time so that the problem of optimal occupation of the neighbour OH sites could be avoided. In the case of HABW, which has a smaller number of atoms per UC, we also considered, for comparison, the optimisation of all atomic co-ordinates (21 variables). The optimisations were carried out using the Polak–Ribiere algorithm, recently implemented in the manner suggested by Civalleri et al. [23], with energy convergences of 10^{-3} kcal/mol. The minimal STO-3G basis set was chosen in order to handle a reasonable number of atomic orbitals per UC, hence leading to moderate computing times. Using the optimised geometry, single point calculations were then performed with the ps-21G*(Al, Si)/6-21G*(O, H) basis set (named hereafter as ps-21G*) in order to get the distributed atomic moments, nuclear quadrupole coupling constants, and EFG tensor elements of the O atoms as implemented in the CRYSTAL code [5].

With the ps-21G* basis set, the SCF scheme converged properly for all five zeolites. The exponents used for the 3sp′ orbitals of Si and Al were 0.12339 and 0.17 a.u.$^{-2}$, respectively, and that for the 2sp′ of O was 0.28 a.u.$^{-2}$. The exponents for the d polarisation functions of Si, Al, and O were optimised as 0.5, 0.45, and 0.6 a.u.$^{-2}$, respectively. A standard value of 1.1 a.u.$^{-2}$ was taken for the sp polarisation function on H.

All computations with the CRYSTAL95 code were carried out on an IBM 15-node (120 MHz) Scalable POWERparallel platform (with 1 Gb of memory/CPU). In all cases, the thresholds for the calculations were fixed to 10^{-5} for the overlap Coulomb, the penetration Coulomb, and overlap exchange, to 10^{-6} and 10^{-11} for the pseudo-overlap exchange, and to 10^{-5} for the pseudo-potential series for all levels of basis sets. A typical total geometry optimisation of one bridged Brönsted centre (12 variables) with the STO-3G basis set took 2–3 days on the above cited CPU. The single point computations with the split-valence basis were executed directly without keeping the bielectronic integral files. The respective shortest SCF convergence (seven to eight cycles) took around 1.5–2 h in the case of the Brönsted centres of the HABW zeolite.

3. Results and discussion

3.1. Optimisation of the structures

The optimised parameters regarding two atoms (O, H), four atoms (O, H, Si, Al), and all framework

Table 2
Geometry of the Brönsted sites (distances in Å, angles in °) for HABW optimised with the STO-3G basis set, *N* being the number of different atoms whose co-ordinates were optimised: $N = 2$ corresponds to O and H, 4 is for O, H, Si, and Al[a]

Parameters	*N*				
	1[b]	2[c]	2[d]	4	All
Si–O–Al	124.84	123.81	123.10	126.22	127.92
O–H	0.980	0.975	0.973	0.980	0.980
Si–O	1.648	1.686	1.695	1.764	1.752
Al–O	1.757	1.735	1.738	1.832	1.804
β[e]	1.2	1.1	2.7	3.5	2.5
Si–O–H	115.1	113.2	120.6	113.1	113.5
Al–O–H	120.0	123.0	116.2	120.6	118.5
$\Delta U_{\text{STO-3G}}$	51.7	48.7	46.7	11.4	0.0

[a] Relative energies in kcal/mol.
[b] Only H co-ordinates were optimised with a "rigid" framework obtained from XRD [18] for the LiABW form.
[c] Initial co-ordinates correspond to case (b).
[d] Initial co-ordinates correspond to "cluster" model $R_{\text{OH}} = 0.980$ Å, $R_{\text{SiO}} = 1.734$ Å, $R_{\text{AlO}} = 1.783$ Å obtained by optimisation of the O and H co-ordinates using a procedure analogous to the DLS fitting with some weights for the fitted parameters.
[e] β is the angle of H deflection from the Si–O–Al plane.

Table 3
Geometry of the Brönsted sites (distances in Å, angles in °) for HABW optimised with the STO-3G basis set varying the co-ordinates of the H, O, Si, and Al atoms[a]

Parameters	HABW[b]			
	O(2)	O(3)	O(4)	O(1)
Si–O–Al initial	139.45	124.87	124.84	143.34
Si–O–Al optimised	139.06	126.37	126.22	143.32
O–H	0.981	0.979	0.980	0.982
Si–O	1.745	1.768	1.764	1.790
Al–O	1.809	1.828	1.832	1.861
Al–H	2.350	2.457	2.480	2.371
β[c]	9.7	10.4	3.5	16.3
Si–O–H	110.0	113.7	113.1	106.1
Al–O–H	112.0	118.9	120.6	109.1
$\Delta U_{\text{STO-3G}}/\Delta U_{\text{ps-21G*}}$	0.0/0.0	8.8/0.9	12.3/3.0	22.8/41.4

[a] Relative energies (in kcal/mol) are also given for the ps-21G*(Al, Si)/6-21G*(H, O) basis set.
[b] Initial co-ordinates from [18].
[c] β is the angle of H deflection from the Si–O–Al plane.

atoms of HABW are compared in Table 2. A slightly smaller Si–O–Al angle is usually observed when varying the co-ordinates of the bridged group with fixed Si and Al positions (cases 2[c] and 2[d] in Table 2) compared to the totally optimised geometry (case "All"). Both models in cases 2[c] and 2[d] were built starting from different initial co-ordinates and resulted in a smaller Si–O and Al–O anisotropy (0.04–0.05 Å) compared with what is usually obtained from cluster computations (around 0.2 Å [6]) and recently from periodic studies on the H-forms of the EDI framework (0.13–0.18 Å) [24]. The optimisation of the positions of the O, H, Si, and Al atoms (case $N = 4$) led to a Brönsted centre geometry which nearly corresponded to that produced by total optimisation disregarding the cell parameters (case "All"). Consequently, all types of Si–O(H)–Al moiety for each H-form were further studied after optimising the positions of the four O, H, Si, and Al atoms (Tables 3–5).

We compared the total charges for all optimised and non-optimised TO_4 tetrahedra presenting real building zeolite units (absolute TO_4 charge values are shown in Fig. 1). The number of crystallographically independent TO_4 tetrahedra within the five studied zeolites is 36 (16 non-optimised units — circles and 20 optimised ones — triangles) and 20 (all optimised — squares) for Si and Al, respectively. Interestingly, the optimisation led to a decrease in the total SiO_4 charge. Only four SiO_4 units (triangles) of the HCHA zeolite, not optimised herein, were "incorporated" into the group (|charge SiO_4| $< 2.1|e|$) of the "relaxed" Si atoms (circles). These SiO_4 units in the initial HCHA model were optimised by Teunissen [20] using an empirical shell model, which could explain their lower charges.

In accordance with XRD data, most of the zeolites possess a distorted TO_4 tetrahedra whose analyses could be useful in order to understand its influence on the relative stability of different zeolite forms. More particularly, it is convenient to study distortions of TO_4 in terms of the symmetry co-ordinates. The latter are zero for a straight T_d symmetry and increase as the tetrahedra deviate from T_d symmetry. Both the valence and deformational types correspond to the rows of the irreducible representation of the F_2 type within the T_d point symmetry group, that is, the stretching (valence) distortions $\Delta s = \max(a_i - a_j)$, $i, j = 1$–3, where $a_1 = \Delta r_1 + \Delta r_2 - \Delta r_3 - \Delta r_4$, $a_2 = -\Delta r_1 + \Delta r_2 + \Delta r_3 - \Delta r_4$, and $a_3 = \Delta r_1 - \Delta r_2 + \Delta r_3 - \Delta r_4$, in which $\Delta r_k = (r_k - R)$ is the displacement length of the *k*-atom from the average value $R = \left(\sum r_m\right)/4$; and the angular (deformational) distortions $\Delta d = \max(b_i - b_j)$, $i, j = 1$–3, wherein $b_1 = \Delta\alpha_{12} - \Delta\alpha_{34}$,

Table 4
Geometry of the Brönsted sites (distances in Å, angles in °) for HEDI and HCHA optimised with the STO-3G basis set varying the co-ordinates of the H, O, Si, and Al atoms[a]

Parameters	HEDI[b]				HCHA[c]			
	O(3)	O(4)	O(2)	O(1)	O(8)	O(2)	O(5)	O(7)
Si–O–Al initial	134.76	138.27	132.47	143.38	130.70	145.55	142.68	143.08
Si–O–Al optimised	135.41	129.10	142.00	139.26	138.68	145.89	143.35	141.92
O–H	0.970	0.983	0.971	0.983	0.971	0.983	0.973	0.971
Si–O	1.775	1.827	1.746	1.676	1.740	1.716	1.750	1.719
Al–O	1.845	1.906	1.829	1.913	1.839	1.820	1.883	1.929
Al–H	2.396	2.493	2.353	2.463	2.39	2.26	2.40	2.47
β[d]	3.7	0.3	1.2	0.4	4.2	12.6	15.2	16.3
Si–O–H	111.6	115.3	107.5	108.2	108.1	110.3	105.1	106.1
Al–O–H	112.9	115.6	110.5	112.5	113.1	103.0	110.3	109.1
$\Delta U_{\text{STO-3G}}/\Delta U_{\text{ps-21G*}}$	0.0/0.0	15.4/14.1	16.1/34.2	62.4/59.3	0.0/0.0	16.0/51.0	76.7/72.0	80.1/76.3

[a] Relative energies (in kcal/mol) are also given for the ps-21G*(Al, Si)/6-21G*(H, O) basis set.
[b] Initial co-ordinates from [21].
[c] Initial co-ordinates from [20].
[d] β is the angle of H deflection from the Si–O–Al plane.

$b_2 = \Delta\alpha_{23} - \Delta\alpha_{14}$, and $b_3 = \Delta\alpha_{13} - \Delta\alpha_{24}$, in which α_{kl} is the O_k–T–O_l angle between the bonds with the k- and l-oxygen neighbours of each T atom (k, l = 1–4) and $\Delta\alpha_{kl} = \alpha_{kl} - 109°47'$ (Fig. 2). Higher valence distortions Δs were observed with higher deformational distortions Δd. Such a correlation shows the usual distortion of the TO_4 tetrahedra with respect to both the valence and angular co-ordinates. This tendency can be more clearly seen for the AlO_4 tetrahedra (Fig. 2) owing to the fact that all AlO_4 units were relaxed in the course of the optimisation.

The models of the bridged Brönsted centres optimised herein include a variety of bridged types, in terms of the Si–O and Al–O bond lengths, comparable to those usually obtained with isolated cluster models [6]. The variations among the Si–O–Al, T–O–H angles, and T–O distances (T = Al, Si) related to the bridged moiety are moreover remarkable among

Table 5
Geometry of the Brönsted sites (distances in Å, angles in °) for HCAN and HNAT optimised with the STO-3G basis set varying the co-ordinates of the H, O, Si, and Al atoms[a]

Parameters	HCAN[b]				HNAT[c]			
	O(3)	O(4)	O(2)	O(1)	O(4)	O(2)	O(3)	O(1)
Si–O–Al initial	135.43	148.59	149.98	135.41	135.80	129.44	139.33	141.19
Si–O–Al optimised	135.03	148.84	149.08	136.51	139.00	124.22	126.37	141.53
O–H	0.981	0.976	0.985	0.975	0.981	0.979	0.974	0.981
Si–O	1.768	1.743	1.817	1.730	1.772	1.730	1.767	1.687
Al–O	1.840	1.818	1.899	1.854	1.836	1.796	1.860	1.884
Al–H	2.44	2.28	2.40	2.35	2.34	2.29	2.38	2.39
β[d]	1.0	3.9	14.4	35.2	28.0	10.4	25.2	13.9
Si–O–H	108.6	106.0	101.5	106.7	107.1	107.1	105.3	108.6
Al–O–H	116.3	105.1	108.4	108.6	108.9	108.2	110.4	108.7
$\Delta U_{\text{STO-3G}}/\Delta U_{\text{ps-21G*}}$	0.0/0.0	3.1/12.6	31.7/61.0	40.6/66.1	0.0/15.4	2.6/30.3	6.6/0.0	58.6/36.4

[a] Relative energies (in kcal/mol) are also given for the ps-21G*(Al, Si)/6-21G*(H, O) basis set.
[b] Initial co-ordinates from [19].
[c] Initial co-ordinates from [22].
[d] β is the angle of H deflection from the Si–O–Al plane.

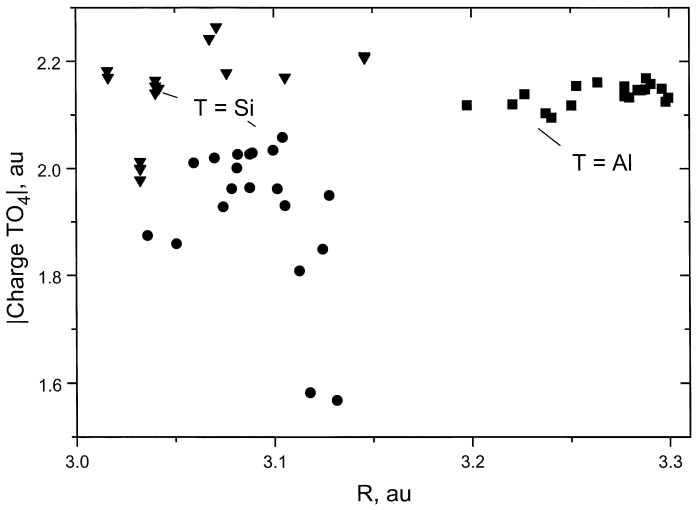

Fig. 1. Absolute total TO_4 charge value (in a.u.) for each crystallographically independent type of TO_4 tetrahedra optimised within the five H-form aluminosilicates at the ps-21G* level with respect to average T–O distance R (in Å): T = Si, non-relaxed unit (▼); T = Si, relaxed unit (●); T = Al, relaxed unit (■).

the various structures, i.e. the differences between the Al–O and Si–O bonds range between 0.06 Å for HABW and 0.24 Å for HEDI. The angles and bond distances nearly correspond to isolated cluster models [6], such as O(1) in HEDI, O(7) in HCHA, and O(1) in HNAT. Very close models with lower Si–O and Al–O anisotropy have also been optimised with the plane wave method [7] and for the O(3) centre in HEDI as optimised with a semi-empirical scheme [24]. The consideration of this variety of bridged type is very important in order to be sure that the analysis of the lower moments presented below either is valid

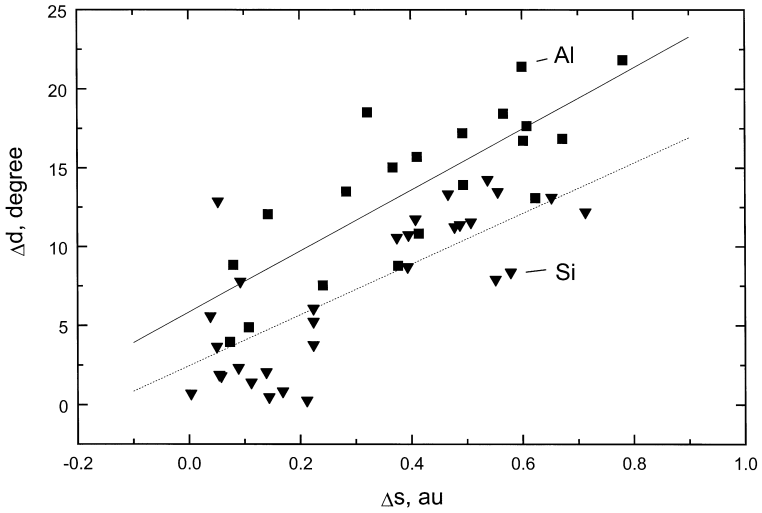

Fig. 2. Correlation between the deformational distortion (in °) $\Delta d = \max(b_i - b_j)$, $i, j = 1$–3, b_i being the angular co-ordinate, and the valence distortion (in a.u.) $\Delta s = \max(a_i - a_j)$, $i, j = 1$–3, a_i being the valence co-ordinate, for each crystallographically independent type of TO_4 tetrahedra optimised at the ps-21G* level within the five H-form aluminosilicates: T = Si (▼/···); T = Al (■/—).

for all considered cases or would require some corrections. The optimised geometry for the most favoured H sites for all frameworks can be crudely described by Si–O distances of 1.74–1.77 Å, Al–O distances of 1.83–1.85 Å, and H–O distances of 0.97–0.98 Å. The favoured resulting bridged models thus present smaller differences between the Al–O and Si–O bond lenghts than the models coming from isolated cluster calculations [6]. Generally, the Si–O–Al angles remain close to those measured by XRD on the cationic forms [18,19,21,22], which were used as the starting H positions in our optimisations (Tables 2–5). Either a decrease or an increase of the Si–O–Al angle was observed relative to the initial value at the preferential position for the bridged H atom. Al–H distances of all optimised models ranged between the experimental NMR estimations, 2.37 ± 0.04 and 2.48 ± 0.04 Å, assigned to the OH positions in the six-membered rings and large cages of the HY zeolite, respectively [25].

The order of the relative energies for the different H sites within the same zeolite form given by the STO-3G optimisation coincided with those obtained by single point calculations with ps-21G*, with the exception of HNAT. In some cases, the ps-21G* calculations led to even higher differences in the relative energies between the sites of the same H-form than those obtained from the STO-3G optimisation. Comparing the relative energy values for different sites within the same zeolite form with those previously obtained [2,6,7,24], our calculations usually produced larger differences. The larger energy differences are due either to the non-complete relaxation of the structure or to the use of the minimal STO-3G basis set for the optimisation.

The H-form of the EDI framework obtained herein can also be compared with the recent results by Ugliengo et al. [24]. Their geometry for all the bridged models differs as compared to our results for the different H positions. Their results are very close to the cluster results mentioned above [6], mainly because the semi-empirical optimisation method they used was parameterised in accordance with data from cluster DFT calculations.

3.2. Approximation of the Mulliken atomic charges

Approximate functions for the evaluation of the atomic charges versus the internal co-ordinates of the framework atoms obtained by analysing the "small" size zeolites could evidently be applied to zeolite models having a "larger" number of atoms per UC or models with non-ordered locations of the substituting atoms in the UC. This strategy is useful when the usual approaches for estimating the long range interactions are difficult to apply. The search for such functions for complicate systems such as the H-form zeolites requires a preliminary discussion regarding more simpler materials. In previous studies, we fitted the Mulliken charges of all types of crystallographic independent O atom included into 13 all-siliceous zeolite frameworks [9–11] as well as the charges on the Al–O–P type oxygens within 12 ALPOs [12]. A two-dimensional function with respect to the average Si–O distance (R) and Si–O–Si angle (ϑ) was derived for the oxygens within the all-siliceous zeolites with a root mean square deviation (RMSD) between the calculated and approximated values of 1.23% using the ps-21G*(Si)/6-21G*(O) basis set. An additional third variable, the bond anisotropy, $\Delta R = R_{\mathrm{AlO}} - R_{\mathrm{PO}}$, allowed to represent the O charges within the ALPO structures with an RMSD = 1.55% at the same basis set level [12]. Here, we tried to fit an analogous three-dimensional function for the O charges in H-forms, with six parameters

$$Q_0^0(R, \Delta R, \vartheta) = a_1 \mathrm{e}^{nR} + a_2 \mathrm{e}^{m[(\Delta R - R_0)]} \times \cos(\vartheta - \vartheta_0) \quad (1)$$

This function was found to be satisfactory for all three Si–O(H)–Al, Si–O–Al, and Si–O–Si cases (the last Si–O–Si moiety is present in the CHA, EDI, and NAT only) with RMSD = 1.14, 0.85, and 0.84%, using 20, 60, and 24 crystallographically independent O atoms, respectively (Table 6). It should be noted that the differences between the minimal and maximal charge values were around 6.6, 6.2, and 4.4% of the maximal charge value within each of the three types of moiety.

Evidently, function (1) has an "effective" character in the case of the Si–O(H)–Al moiety because it does not take into account the co-ordinates related to the H position with respect to the closest O and Si atoms. That is why, for Si–O(H)–Al, we also tested a modification of function (1), which included an additional isotropic dependence $a_3 \mathrm{e}^{kR'}$, where $R' = R_{\mathrm{OH}}$ or R_{SiH}. The distance R_{SiH} could be related to a charge transfer from the H to the Si atom (which should

Table 6
Parameters of the approximate function (Eq. (1)) evaluated from the calculation with the ps-21G* basis set of the N charges of all crystallographically independent O types for the different T–O–T′ moieties within all five H-form aluminosilicates

Type	N	A_1	n	A_2	R_0 (Å)	m	ϑ_0 (rad)	RMSD (%)
Si–O(H)–Al	20	1.389	−0.161	0.361	0.699	0.568	−0.607	1.14
	20[a]	1.391	0.098	0.510	0.466	−0.212	0.740	1.11
Si–O–Al	60	2.444	−0.509	−0.030	0.497	−1.773	3.440	0.85
Si–O–Si	24	1.270	−0.145	8.827	0.464	1.274	0.682	0.84

[a] Parameter $a_3 = 0.883$, $k = 0.783$ for eight-parameter function (1) including also $a_3 e^{kR'}$ with $R' = R_{OH}$.

influence the nearest O charge) as it had been suggested by the close band positions of the H and Si atoms in the projected density of states of H-sodalite calculated by Nicholas and Hess [25]. However, their H-sodalite model considered relatively shorter Al–O and Si–O distances compared to those determined theoretically using a cluster model [6] and experimentally from NMR measurements [26]. Hence, a longer Si–H distance could explain the insensitivity observed here to the Si–H distance for the charge of the bridged O in the series of optimised H-forms. Indeed, only a slightly better RMSD = 1.11% was obtained when fitting with $R' = R_{OH}$, $a_3 = 0.883$, and $k = 0.783$. This minor RMSD decrease could be explained by the very small variation of the OH bond length throughout all H-form models.

An important application of the charge dependences with respect to the approximations considering higher order multipole moments is the subject of another paper [27]. At this stage, it can be said that the inclusion of the differences between the first neighbour O charges as presented by dependence (1) is extremely important for constructing the approximations for the higher order moments of the Si and Al atoms in the same series of H-forms. For example, such approximation for the small atomic dipoles of the Si and Al atoms within slightly distorted tetrahedra TO_4 cannot be obtained if we consider equal (or averaged) charges for the O neighbours. The higher the moment, the lower the influence of the approximate co-ordinate of the lower moments on the resulting fitting of the higher moments. Specifically, the influence of the charge approximation on the octupole moment approximation is very minor. Hence, this paper presents the first step necessary for the general development of approximations of all higher multipole moments required to compute precise values for the electrostatic potential.

3.3. Approximation of the oxygen dipole moments

Irrespective of the scheme for the electron density partition (atomic centres only or atomic and bond centres), complementing the atomic charges by higher multipole terms will lead to a more precise estimation of the electrostatic field. The importance of the dipole and quadrupole terms has already been shown for the adsorption of CO over a TiO_2 slab [28]. This importance is illustrated here by comparing the electrostatic potential (EP) values obtained with the ps-21G* basis set (Fig. 3a) with the EP representation at three different levels based on the neglection of parts of the atomic multipole moments in the case of the HCHA framework. Generally, the inclusion of the moments up to fourth order should be sufficient for a correct calculation of the EP [6]. The three levels of the EP evaluation included Mulliken charges ($L = 0$ in Fig. 3b) on all atoms, charges and dipoles ($L = 0$ and 1 in Fig. 3c) on all atoms, and all atomic moments up to third order ($L = 3$ in Fig. 3d). Looking at EP differences in relation to spatial co-ordinates is more significant than the EP values only because it provides a clearer separation between the various field approximations. The EP maps were calculated in the Si(2)–O(2)–Al plane of the HCHA framework (Fig. 3a, where the co-ordinates of O(2) are $x = 17$ a.u. and $y = 17$ a.u.) applying the POTM option available in CRYSTAL95 [5]. As soon as the EP value of any other atom displaced from the plane is lower than the one of the Si(2), O(2), and Al atoms, the other atoms can be looked at a better resolution. In order to visualise the allowed space "within the plane", the all EP scale ranges from −0.007 to 2.0 a.u. The space around the Si(2)–O(2)–Al moiety was expanded by 8 Å (15.12 a.u.) in order to show the EP behaviour within an area available for a small adsorbed molecule. From this view, one immediately

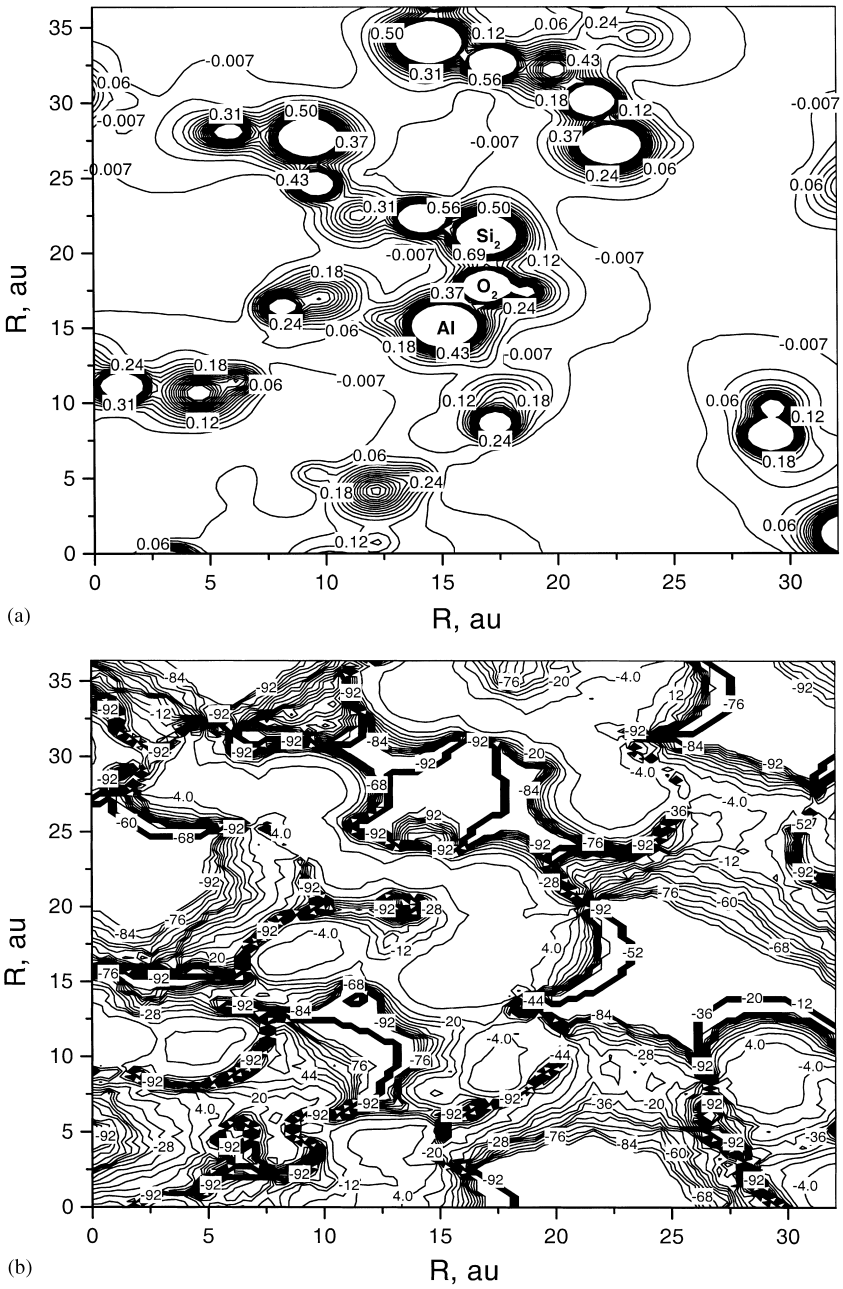

Fig. 3. Electrostatic potential (a) values EP(L) (in a.u.) and EP differences presented as (1-EP(L)/EP(6)) × 100 (%) obtained with (b) Mulliken charges ($L = 0$) on all atoms, (c) charges and dipoles ($L = 0$ and 1) on all atoms, and (d) all atomic moments up to third order ($L = 3$) relative to the potential representation based on the sixth order moments ($L = 6$). The moments are calculated at the ps-21G* level with respect to the Si(2)–O(2)–Al plane of the HCHA framework. L value corresponds to the upper atomic moment considered for the EP calculation.

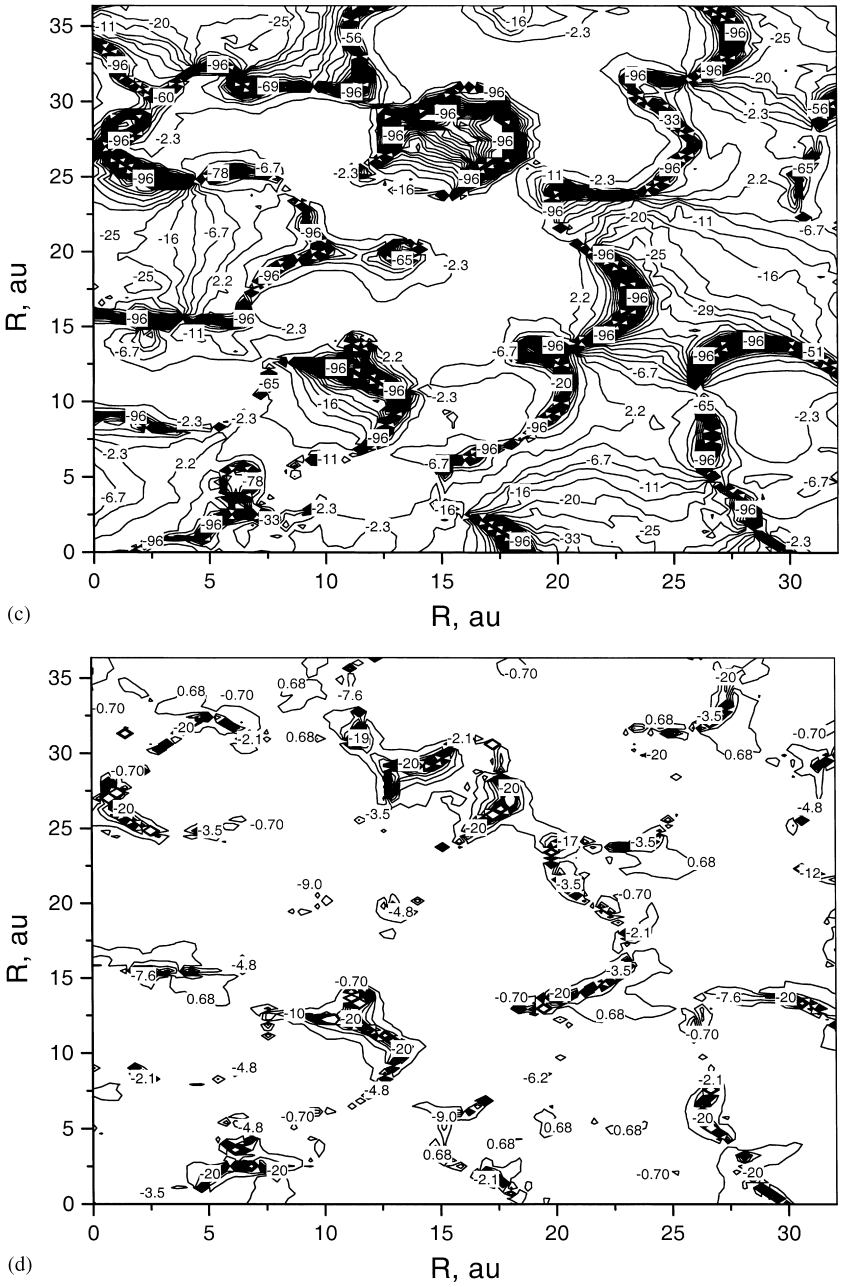

Fig. 3 (*Continued*).

notices that a small adsorbed molecule can be located in the left side (centred around $x = 0$ a.u. and $y = 5$ a.u. or $x = 0$ a.u. and $y = 20$ a.u., respectively, in Fig. 3a) and right lower corner (centred around $x = 25$ a.u. and for y ranging between 0 and 20 a.u.) between the framework atoms located relatively close to the plane passing through one of the four tetrahedral rings of the HCHA framework.

Comparing Fig. 3b–d, one can see that the EP differences (1−EP(L)/EP(6)) are large along the line EP(6) = 0 a.u. (see contour line −0.007 a.u. close to 0 a.u. in Fig. 3a) with all three levels of computation (Fig. 3b–d). This cannot, however, be considered as a drawback of the three representations because even a negligible shift from EP = 0 a.u. should lead to a sharp EP difference. Then, there are large differences between the "$L = 0$" and "$L = 0$ and 1" evaluations of the EP difference maps in the above mentioned available part of framework internal space (Fig. 3b and c). The EP evaluations allowing dipole moments (case c) are usually three to four times better than those disregarding them within the same space. The EP map corresponding to the moments up to second order is not presented as it is only slightly better than the "$L = 0$ and 1" EP map. There is, however, a sharp improvement in the map when adding octupole moments as in case (d), which could be explained by the relatively higher contributions of the third order moments of the Al and Si atoms. For their configurations, which are close to tetrahedral ones, permanent non-zero electrostatic moment values lower than octupoles are forbidden.

The absolute value of the atomic dipole moment can be expressed as

$$Q_1 = ((Q_1^0)^2 + (Q_1^1)^2 + (Q_1^{-1})^2)^{1/2} \quad (2)$$

where Q_L^m is the m-component of the L-order atomic multipole moment (e a.u.^{L}), within the Mulliken partition scheme of the calculation method of the multipole moments proposed by Saunders et al. [4]. The O dipole values Q_1 are approximated using a two-parameter function

$$Q_1(\vartheta) = c \sin(\vartheta - \vartheta_0) \quad (3)$$

where c and ϑ_0 are given in Table 7. The RMSD values between the calculated and approximated O dipole moments for the Si–O–Si, Si–O–Al, and Si–O(H)–Al oxygen types are 4.44, 4.65, and 11.50%, respectively. These rather higher RMSD values as compared to the RMSDs for the respective O charges (around 1%, see Section 3.2 and Table 6) should be considered in a wider range of dipole variations being near 51, 30, and 48%, for Si–O(H)–Al, Si–O–Al, and Si–O–Si, respectively. The ranges of the dipole variation were estimated as the difference between the extremal values divided by the maximal one.

Table 7
Parameters of the approximate function (Eq. (3)) evaluated from the calculation with the ps-21G* basis set of the N dipoles of all crystallographically independent O types for the different T–O–T′ moieties within all five H-form aluminosilicates

Type	N	C	ϑ_0 (rad)	RMSD (%)
Si–O(H)–Al	20	0.2475	−0.0883	11.50
Si–O–Al	60	0.2895	0.1120	4.65
Si–O–Si	24	0.3176	0.0394	4.44
Si–O–Si[a]	19	0.2516	0.0233	5.37

[a] For all-siliceous zeolite frameworks [9,10].

A six-parameter function, first proposed for the O dipole moments in a series of 12 ALPOs was hence also applied to the H-forms studied

$$Q_1(R, \Delta R, \vartheta) = a_1 e^{n\,\Delta R} + a_2 e^{m(R-R_0)} \times \sin(\vartheta - \vartheta_0) \quad (4)$$

yielding slightly better RMSD values of 10.16 and 4.23% only for the Si–O(H)–Al and Si–O–Si oxygens, respectively (Table 8). As far as involving more complicated terms proportional to R and ΔR does not lead to a higher quality fit, the simple *sine* function (Eq. (3)) deserves closer attention. The dominant influence of the T–O–T′ angle on the O dipole was observed earlier in the ALPO structures with the ps-21G* basis set [12] (Fig. 4). A similar variation of the O dipole with the Si–O–Si angle at the ps-21G* basis set level can be observed between the H-forms and all-siliceous forms (Fig. 5). In this figure, we present first the 106 absolute dipole values of all crystallographically independent types of oxygen for all 13 all-siliceous zeolites considered in our previous paper at the STO-3G level [9] (diamonds in Fig. 5) along with the 19 dipole values of five zeolites (i.e. CHA, GME, MER, MON, RHO) calculated with ps-21G* [10] (squares in Fig. 5). Using the same *sine* character function for all O types versus the Si–O–Si angle, the dipoles within all-siliceous forms present lower values than those of the same type within the H-forms. In order to explain this, let us consider the multipoles in terms of an "isolated" three-atom moiety whose central dipole moment is related to the O atom. The contribution to the moment from each of the T–O bond

Table 8
Parameters of the approximate function (Eq. (4)) evaluated from the calculation with the ps-21G* basis set of the N dipoles of all crystallographically independent O types for the different T–O–T′ moieties within all five H-form aluminosilicates

Type	N	a_1	n	a_2	R_0 (Å)	m	ϑ_0 (rad)	RMSD (%)
Si–O(H)–Al	20	0.177	0.784	0.2201	0.995	0.097	−0.107	10.16
Si–O–Al	60	0.718	2.883	0.1475	−1.14	0.649	0.1173	4.59
Si–O–Si	24	0.125	1.203	0.3903	1.35	0.168	0.038	4.23

dipoles will be lower for the Si–O–Al case because the longer Al–O bond length, compared to that of Si–O, leads to a smaller effect as compared to the decrease in the Al charge (1.70–1.77 $|e|$), compared to the Si charge (1.8–2.0 $|e|$). One could certify that this difference is not a consequence of the optimisation of the co-ordinates of the oxygens because the dipole values of relaxed and non-relaxed O atoms are equally close to the approximation $c\sin(\vartheta - \vartheta_0)$ given by the dashed line in Fig. 5.

The knowledge of the geometry only allowed us to obtain satisfactory approximations of the absolute value of the O dipole moment only. Considering also the charges on the neighbour atoms (for example, as recommended for Si in [10,11]), one could develop a more general relation for each component of the O dipole. This work is in progress [27].

3.4. Electrostatic field gradient and ^{17}O nuclear quadrupole coupling constants

One of the interesting options of the CRYSTAL code is the possible detailed analysis of the electrostatic field value. 3D periodic conditions considered in the course of the Hartree–Fock solution allow the estimated electrostatic potential and its derivatives to be used as the source data for the electrostatic field within potential-oriented and cluster computations. The EFG is one of the important factors which governs the deprotonation energy [2] on the one hand, and influences the NMR spectra of the quadrupolar ^{17}O nuclei [13–15] on the other. The EFG values obtained herein with CRYSTAL95 (Fig. 6) using the ps-21G* basis are positive for the Si–O–Al and Si–O–Si oxygens and negative for the Si–O(H)–Al ones, as a consequence

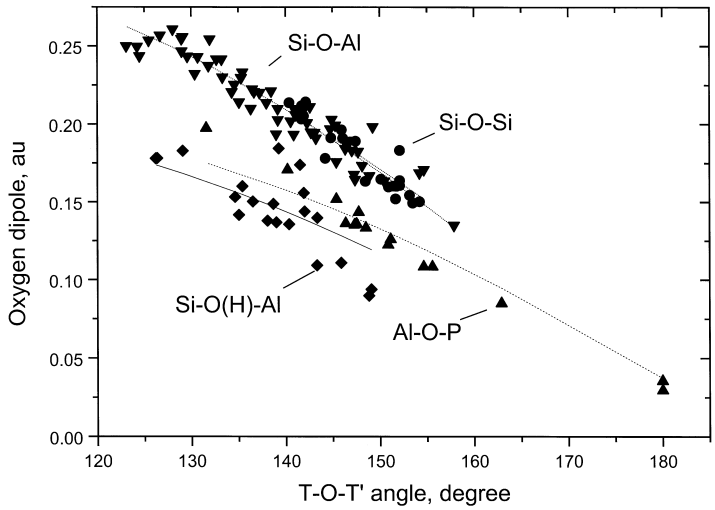

Fig. 4. Approximations of the O dipole moments of the Si–O(H)–Al (◆), Si–O–Si (●), and Si–O–Al (▼) moieties in the H-form aluminosilicates and ALPO (▲) calculated at the ps-21G* level using the $c\sin(\vartheta - \vartheta_0)$ function. Approximations via *sine* functions are given by solid (—), dotted (···), dotted-dashed (·-·-·), and dashed (- - -) lines, respectively.

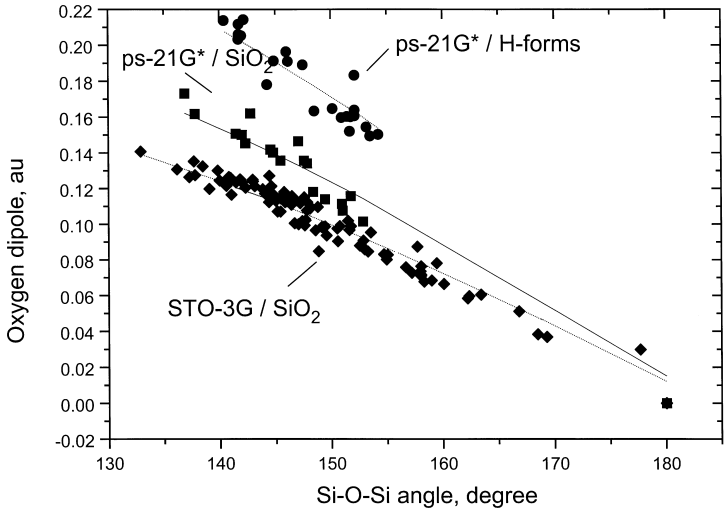

Fig. 5. Approximations of the O dipole moment for the Si–O–Si moieties within the H-form aluminosilicates calculated at the ps-21G* level (●) and all-siliceous zeolites calculated at the STO-3G (◆) and ps-21G* (■) levels using the $c\sin(\vartheta - \vartheta_0)$ function. Approximations via *sine* functions are given by dotted (···), dotted-dashed (·-·-·), and solid lines (—), respectively.

of the contribution from the close H atom to the field value ($\nabla E_{zz} < 0$). The EFG values of the Si–O–Si types of oxygen are usually larger than those of the Si–O–Al ones, which has an evident "local" origin. The shorter Si–O distance associated with a higher Si charge compared with the longer Al–O distance with a lower Al charge results in a higher field and EFG value for the Si–O–Si types of oxygen. All three types of moiety show a slight increase in the EFG value in absolute terms as the T–O–T′ bond angle increases. For

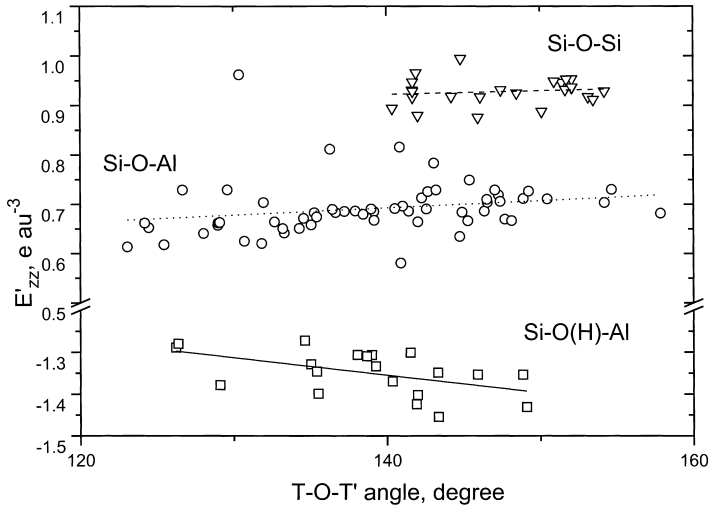

Fig. 6. ^{17}O electrostatic field gradient ∇E_{zz} (e a.u.$^{-3}$) for the Si–O(H)–Al (□), Si–O–Al (○), and Si–O–Si (▽) type O atoms vs. the T–O–T′ bond angle (in °) calculated at the ps-21G* level for all five H-form aluminosilicates. Approximations via linear functions are given by solid (—), dotted (···), and dashed (- - -) lines, respectively.

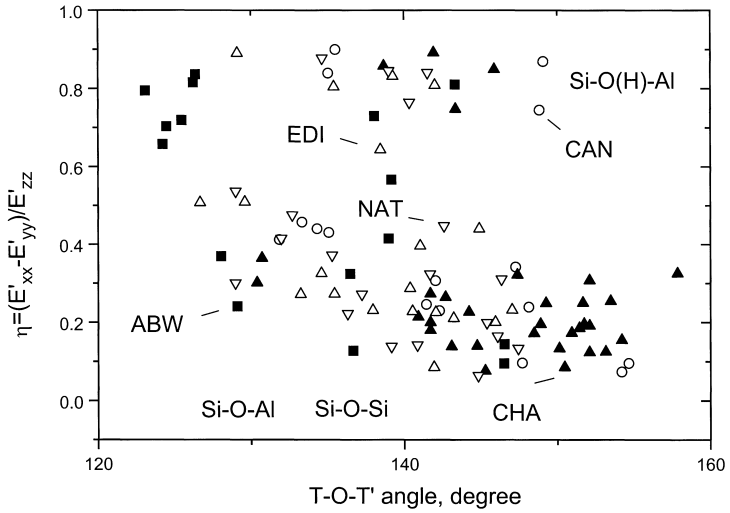

Fig. 7. ^{17}O gradient field anisotropy $\eta = (\nabla E_{xx} - \nabla E_{yy})/\nabla E_{zz}$ vs. the T–O–T′ bond angle (in °) calculated at the ps-21G* level for all five H-form aluminosilicates: HABW (■); HCHA (▲); HCAN (○); HEDI (△) and HNAT (▽).

comparison with known data, it should be mentioned that the smaller absolute ∇E_{zz}(O) determined from XRD measurements within α-Al_2O_3 (between 0.04 and 0.21 e a.u.$^{-3}$) [16,29,30] and nuclear quadrupole resonance (NQR) (0.36 e a.u.$^{-3}$) [31] could be explained by the higher number of closer neighbours and the symmetric location of the Al neighbours in the oxide lattice.

Another parameter which influences the spectra of nuclei having quadrupolar nuclear moments is the EFG anisotropy

$$\eta = \frac{\nabla E_{xx} - \nabla E_{yy}}{\nabla E_{zz}} \tag{5}$$

wherein all EFG elements are related to the EFG tensor principal axes. η does not reveal any difference between the Si–O–Al and Si–O–Si types of oxygen (Fig. 7). This main group of η values is below 0.4. Only the O atoms of the Si–O(H)–Al moiety are characterised by higher η values around 0.9.

The nuclear quadrupole coupling constant C_{qcc} is one of two parameters (together with η) characterising quadrupole interactions of an asymmetric nucleus. The quality of the 6-31G* basis set for the calculation of the NMR characteristics was shown to be good enough by Rohlfing et al. [32] for ^{13}C. The C_{qcc} values (in MHz) for the O atoms within the five H-forms were obtained here using the EFG values at the O positions (Fig. 6)

$$C_{qcc} = 2.34 \times 10^2 q \nabla E_{zz} \tag{6}$$

where the coefficient on the right-hand side corresponds to ∇E_{zz} expressed in e a.u.$^{-3}$, and the nuclear quadrupole moment of ^{17}O, $q = -0.026$ b [33] (1 b = 10^{-28} m^2) (Fig. 8). If another known value of $q = -0.02558$ b [34] is used, all C_{qcc} values are only slightly lowered (in absolute value) compared to those shown in Fig. 8. The *ratio* between C_{qcc} and ∇E_{zz} (Eq. (6)) shows that Figs. 6 and 8 are reciprocally inverted, so that analogous results can be demonstrated either in terms of the zeolite types (Fig. 8), or in terms of the T–O–T′ moieties (Fig. 6). The same linear approximations $\nabla E_{zz} = a \times \vartheta + b$, where a and b values are 7.5×10^{-4}, 1.47×10^{-3}, -4.18×10^{-3} e a.u.$^{-3}$ degree^{-1} and 0.877, 0.4873, -0.7703 e a.u.$^{-3}$ for the Si–O–Si, Si–O–Al, and Si–O(H)–Al oxygens, respectively, as given in Fig. 6 (by dashed, dotted, and solid lines, respectively) can be converted for the C_{qcc} values shown in Fig. 8. Following the EFG behaviour, the C_{qcc} values of the Si–O–Al, Si–O–Si, and Si–O(H)–Al types of oxygen are partitioned from −3.5 to −5, −5 to −6, and 7.5 to 9 MHz, respectively. The absolute values of the second moiety are close to the data, 5.1 to 5.39 MHz, obtained experi-

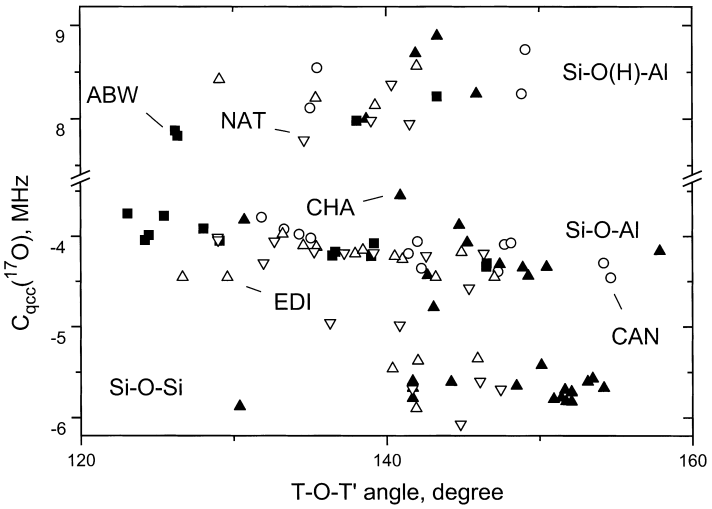

Fig. 8. ^{17}O quadrupole coupling constants C_{qcc} (MHz) vs. the T–O–T′ bond angle (in °) calculated at the ps-21G* level for all five H-form aluminosilicates: HABW (■); HCHA (▲); HCAN (○); HEDI (△) and HNAT (▽).

mentally for all-siliceous faujasite [13], while other experimental data obtained for SiO_2 show values around 5.8 MHz [35]. The positive sign of C_{qcc} mentioned here and below is probably a consequence of the C_{qcc} determination from experimental chemical shift values which depend on the square of the coupling constant. The C_{qcc} values for the Si–O–Al moiety are relatively large compared with the C_{qcc} ones fitted for the NaA and NaLSX zeolites [15], for which most of the estimates were around 3 MHz. Other C_{qcc} data between 2.7 and 5.1 MHz were fitted from double rotation NMR spectra for a series of silicates [31] and 2.2 MHz was obtained from NQR spectra of α-Al_2O_3 [31]. There are no experimental data on the bridged ^{17}O atom connected to a proton. Our calculations, however, show that the respective C_{qcc} for the Si–O(H)–Al types of oxygen should be larger than those for the Si–O–Al moiety which will lead to a broadening of the respective lines in their NMR spectra.

Hence, a relatively good coincidence of C_{qcc} with the known experimental data for the Si–O–Al and Si–O–Si types of oxygen confirms the correct representation of the derivatives of the electrostatic potential on the ^{17}O nuclei using a basis set such as the ps-21G*(Al, Si)/6-21G*(O, H) one with the CRYSTAL95 code. It should be noted that this basis set considers all O electrons including precisely those of the core.

4. Conclusions

Distributed multipole analysis on the basis of periodic Hartree–Fock calculations with the CRYSTAL95 code and the ps-21G*(Al, Si)/6-21G*(O, H) basis set was applied to five H-form aluminosilicate models, which were optimised using the same program at the STO-3G level. Simple analytical functions with respect to the average T–O (T = Si, Al) bond distance, the anisotropy between the Al–O and Si–O bond distances, and the Si–O–Al angle already obtained for the charges and dipoles of all crystallographically independent types of oxygen within a series of ALPO sieves were used to fit the dependences of the Mulliken charges and atomic dipole moments of the O atoms within the H-forms. A marked improvement in the electrostatic potential presentation was observed adding the dipole moments to the charges, considering the space available for small adsorbed probe molecules within the HCHA framework. The domination of the "angular" contribution to the total O dipole was found to coincide with that observed earlier for the O dipoles in the ALPO sieves. The nuclear quadrupole coupling constants for ^{17}O were shown to have a relatively good agreement with the known experimental values for the Si–O–Si and Si–O–Al moieties for different zeolites (A, LSX, Y). It was found that respective nuclear quadrupole coupling constants for the Si–O(H)–Al

type ^{17}O should be appreciably larger in absolute value compared to those for Si–O–Si and Si–O–Al.

Various bridged types of O(H) oxygen were obtained during the optimisations. For all of them, lower order moments demonstrated a common behaviour. The close agreement between the experimental and theoretical quadrupole coupling constants for ^{17}O confirms the reasonable values of the gradient of the electrostatic field calculated for the H-forms studied at this basis set level. Thus, it is proposed that the same behaviour of the charges and dipoles with respect to the internal co-ordinates should be observed for a more advanced basis set too.

Acknowledgements

The authors wish to thank the FUNDP for the use of the Namur Scientific Computing Facility (SCF) Centre, a common project between the FNRS, IBM-Belgium, and FUNDP and MSI for the use of their data in the framework of the "Catalysis and Sorption" consortium. They are grateful for the partial support of the Inter-University Research Program on Reduced Dimensionality Systems (PAI/IUAP 4/10) initiated by the Belgian Government.

References

[1] J.B. Nagy, P. Bodart, I. Hannus, I. Kiricsi, Synthesis, Characterisation and Use of Zeolitic Microporous Materials, DecaGen, Szeged-Szoreg, Hungary, 1998, pp. 148–180.
[2] G. Sastre, D.W. Lewis, J. Chem. Soc., Faraday Trans. 94 (1998) 3049.
[3] W.J. Mortier, S.K. Ghosh, S. Shankar, J. Am. Chem. Soc. 108 (1986) 4315.
[4] V.R. Saunders, C. Freyria-Fava, R. Dovesi, L. Salasco, C. Roetti, Mol. Phys. 77 (1992) 629.
[5] R. Dovesi, V.R. Saunders, C. Roetti, M. Causà, N.M. Harrison, R. Orlando, E. Aprà, CRYSTAL95 1.0, User's Manual, 1996.
[6] J. Sauer, P. Ugliengo, E. Garrone, V.R. Saunders, Chem. Rev. 94 (1994) 2095.
[7] Y. Jeanvoine, J.G. Ángyán, G. Kresse, J. Hafner, J. Phys. Chem. B102 (1998) 5573.
[8] P.A. Jacobs, Catal. Rev. Sci. Eng. 24 (1982) 415.
[9] A.V. Larin, L. Leherte, D.P. Vercauteren, Chem. Phys. Lett. 287 (1998) 169.
[10] A.V. Larin, D.P. Vercauteren, Int. J. Quant. Chem. 70 (1998) 993.
[11] A.V. Larin, D.P. Vercauteren, Int. J. Inorg. Mater. 1 (1999) 201.
[12] A.V. Larin, D.P. Vercauteren, J. Mol. Catal. A, in press.
[13] L.M. Bull, A.K. Cheetham, T. Anupold, A. Reinhold, A. Samoson, J. Sauer, B. Bussemer, Y. Lee, S. Gann, J. Shore, A. Pines, R. Dupree, J. Am. Chem. Soc. 120 (1998) 3510.
[14] J.-P. Amoureux, F. Bauer, H. Ernst, C. Fernandez, D. Freude, D. Michel, U.-T. Pingel, Chem. Phys. Lett. 285 (1998) 10.
[15] U.-T. Pingel, J.-P. Amoureux, T. Anupold, F. Bauer, H. Ernst, C. Fernandez, D. Freude, A. Samoson, Chem. Phys. Lett. 294 (1998) 345.
[16] A.S. Brown, M.A. Spackman, Mol. Phys. 83 (1994) 551.
[17] C. Pisani, R. Dovesi, C. Roetti, Hartree–Fock ab initio Treatment of Crystalline Systems, Springer, New York, 1988.
[18] E. Krogh Andersen, G. Ploug-Sorensen, Zeit. Kristallogr. 176 (1986) 67.
[19] N. Bresciani Pahor, M. Calligaris, G. Nardin, L. Randaccio, Acta Cryst. B38 (1982) 893.
[20] E. Teunissen, Ph.D. Thesis, University of Eindhoven, The Netherlands, 1994.
[21] E. Galli, Acta Cryst. B32 (1976) 394.
[22] F. Pechar, W. Schafer, G. Will, Zeit. Kristallogr. 164 (1983) 19.
[23] B. Civalleri, C.M. Zicovich-Wilson, P. Ugliengo, V.R. Saunders, R. Dovesi, Chem. Phys. Lett. 292 (1998) 394.
[24] P. Ugliengo, B. Civalleri, R. Dovesi, C.M. Zicovich-Wilson, Phys. Chem. Chem. Phys. 1 (1999) 545.
[25] J.B. Nicholas, A.C. Hess, J. Am. Chem. Soc. 116 (1994) 5428.
[26] D. Fenzke, M. Hunger, H. Pfeifer, J. Mag. Reson. 95 (1991) 477.
[27] A.V. Larin, D.P. Vercauteren, Int. J. Quant. Chem., in press.
[28] P. Reinhardt, M. Causà, C.M. Marian, B.A. Heß, Phys. Rev. B54 (1996) 14812.
[29] A. H Silver, T. Kushida, J. Lambe, Phys. Rev. 125 (1962) 1147.
[30] D. Sundholm, J. Olsen, Phys. Rev. Lett. 68 (1992) 927.
[31] E. Brun, B. Derighetti, E.E. Hundt, H.H. Niebuhr, Phys. Lett. A31 (1970) 416.
[32] C. McMichael Rohlfing, L.C. Allen, R. Ditchfield, Chem. Phys. 63 (1981) 185.
[33] K.T. Mueller, Y. Wu, B.F. Chmelka, J. Stebbins, A. Pines, J. Am. Chem. Soc. 113 (1991) 32.
[34] F. Ajzenberg-Selone, Nucl. Phys. A281 (1970) 1.
[35] S. Schramm, R.J. Kirkpatrick, E. Oldfield, J. Am. Chem. Soc. 105 (1983) 2483.